



Analytical model of flow maldistribution in polymer electrolyte fuel cell channels

Suman Basu^{a,*}, Chao-Yang Wang^a, Ken S. Chen^b

^a Electrochemical Engine Center (ECEC), and Department of Mechanical and Nuclear Engineering, The Pennsylvania State University, University Park, PA 16802, USA

^b Engineering Sciences Center, Sandia National Laboratories, Albuquerque, NM 87185-0836, USA

ARTICLE INFO

Article history:

Received 22 February 2010

Received in revised form

23 June 2010

Accepted 27 August 2010

Available online 17 September 2010

Keywords:

Polymer electrolyte fuel cell

Multiphase flow

Flow maldistribution

Mathematical modeling

Porous media

Fluid mechanics

ABSTRACT

Gas–liquid, two-phase flow through channels of a polymer electrolyte fuel cell (PEFC) is of great interest as reactant oxygen is supplied and liquid product water is removed via these PEFC channels. Gas diffusion layer (GDL) intrusion in the channels, which is inherent to the process of PEFC cell and stack assembling, increases the local flow resistance in the intruded channels and consequently lowers their flowrates. This flow maldistribution renders the intruded channels more susceptible to liquid water accumulation or flooding. A one-dimensional analytical model is developed in this work to elucidate the two-phase flow maldistribution in PEFC channels resulting from GDL intrusion. Relative humidity (RH) and the stoichiometric flow ratio of inlet gases are found to be the two key parameters controlling the flow maldistribution in PEFC channels. Interestingly, our analysis shows that decreasing the inlet RH worsens flow maldistribution. As GDL intrusion in channels is inevitable, a good flow-field design must be inherently tolerable to flow maldistribution. Using the analytical model presented herein, the number of flow channels and their U-turns are optimized to minimize the detrimental effect of GDL intrusion.

© 2010 Elsevier Ltd. All rights reserved.

1. Introduction

Polymer electrolyte fuel cells (PEFCs) are rapidly becoming a viable alternative energy or power source for automobile and stationary applications in the emerging hydrogen economy. However, before PEFCs can be employed routinely as power sources, the key phenomena of liquid water transport and removal from gas diffusion layers (GDLs) and channels must be understood. In particular, channel flooding is one of the critical problems faced by the PEFC community today. Partial blockage of gas channels by softer GDL material due to the high assembly pressure for minimizing contact resistance between bipolar plate and GDL is referred to as “GDL intrusion” (Fig. 1). Consequently, more pumping power is required to drive reactant and product flow through the intruded channels. A method to measure in situ gas diffusion layer intrusion in the flow field channels was previously proposed and demonstrated (St-Pierre et al., 2007). The GDL intrusion is most significant in the channels close to the end as the contact pressure reaches its maximum at these locations (Kandlikar et al., 2009). Uneven GDL intrusion redistributes flow in the parallel channels. Although, experimental

investigation of instability induced flow maldistribution in parallel gas channels of a PEFC are available in the literature (Zhang et al., 2008), to the best of the authors’ knowledge, experimental investigation on effect of uneven GDL intrusion on flow distribution in parallel channels of a PEFC does not exist in open literature.

Flow through the intruded channel decreases, which in turn lowers the local stoichiometric flow ratio or simply stoichiometry. At low stoichiometry, the ability to flush liquid water via flow decreases and liquid saturation level thus rises in the channel, thereby exacerbating the mass transport loss and giving rise to operational instabilities due to channel flooding. The maldistribution of flow in parallel channels in itself is detrimental, leading to profound performance and durability deteriorations. Directly, reactant maldistribution leads to non-uniform utilization of the catalyst. The indirect problem is that the intruded channel is more susceptible to blockage by liquid water due to low gas flow rate, which leads to a serious loss of efficiency of the PEFC because the whole channel is now lost due to blockage. Hence, for a PEFC to maintain its stable performance, flooding of the channels must be avoided.

Liquid saturation level can vary widely in the gas channels, thus simple mist flow or film flow models may not be adequate. Multiphase mixture (or M^2) model has been employed to approximate the two-phase flow in the channels (see, e.g., Wang et al., 2008; Basu et al., 2009). Since flow in the channel occurs

* Corresponding author. Present address: India Science Lab, General Motors Technical Center India, ITPL, Bangalore 560066, India.

E-mail address: suman_basu@yahoo.com (S. Basu).

predominantly in the along-channel direction, flow variables in the channel are reduced to three—pressure, velocity along the flow direction and volume fraction of liquid water. Also, the axial diffusion of species is negligible (the Peclet number is found to be of the order of 1000 or more). Therefore, an analytical treatment of the two-phase flow in channels is feasible (Wang et al., 2008).

Channel flooding in PEFCs has received considerable attention recently. A recent review by Anderson et al. (2010), summarizes the efforts to investigate and predict this phenomenon. In the literature analytical solutions for pressure drop due to single-phase flow in PEFC channels are available (see, e.g., Maharudrayya et al., 2005). Maldistribution of single-phase flow due to GDL intrusion in parallel stacks has also been attempted (Rapaport et al., 2006). Investigation of single-phase flow in parallel micro-channels of PEFCs revealed the existence of flow maldistribution (Barrears et al., 2005). Single-phase flow in the channel has been used widely in the gas channel for design purposes (see, e.g., Yoon et al., 2004; Shimpalee et al., 2006; Wang et al., 2007), but experiments (e.g., Yang et al., 2004; Zhang et al., 2006) have shown that flow in PEFC channels is usually not single phase. Therefore, an analytical formula for dry length of a gas channel is an effective design tool (e.g., Wang et al., 2001). An analytical solution exists for predicting liquid droplet instability at the

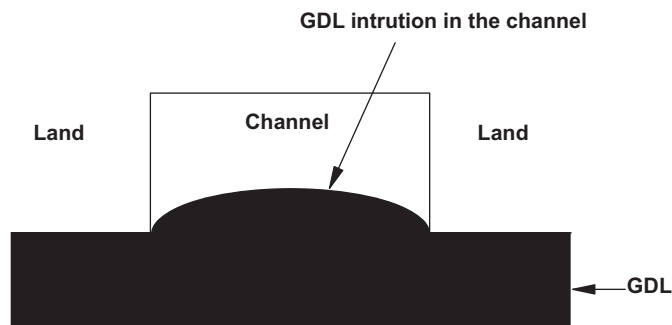


Fig. 1. Schematic of GDL intrusion in a channel.

GDL–channel interface (Chen et al., 2005). Researchers used different conventional two-fluid models to simulate two-phase flow in the gas channels. Although the volume of fluid (VOF) method could be used to explore the droplet growth, stability and movement in the channel (Jiao et al., 2006; Zhu et al., 2008), it is formidably difficult to model full channels in which thousands of droplets of varying length scales are involved. Others used Eulerian two-phase model (e.g., He et al., 2007; Quan and Lai, 2007), which are computationally expensive. The single-fluid two-phase flow models usually assume mist flow (e.g., Yuan and Sunden, 2004), which often in reality is not appropriate.

Although many efforts (experimental, computational as well as analytical) have been undertaken to investigate the flow and transport problem in the PEFC gas channels, none of these provides a simple and efficient model without simplifying the physics of the problem considerably. In this paper, we attempt to construct an analytical model to elucidate two-phase flow maldistribution in the channels using reasonable assumptions without neglecting any significant physics of the two-phase flow.

2. Analytical model

In the present work, we consider a cathode gas channel of a PEFC with 'y' being the flow direction as shown in Fig. 2. To enable an analytical treatment, a constant source term is assumed for both mass and water species. Mass conservation is applied in the control volume covering the entire channel cross-section from $y=0$ to L . Moreover, the following assumptions are made:

- (1) Flow in the channel is taken to occur predominantly in the y direction. That is, mathematically, $\vec{u} = (0, u, 0)$.
- (2) The momentum transfer across the GDL–channel interface is negligible as compared with the momentum due to gas flow in the channel.
- (3) The net water transport coefficient has been reported to be close to zero (Berg et al., 2004). Therefore, it is assumed to be zero.

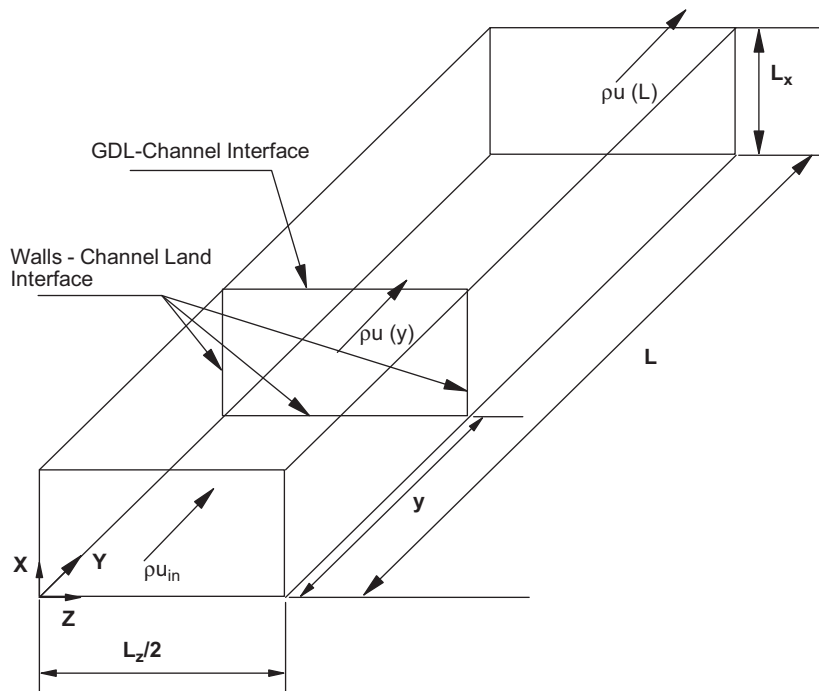


Fig. 2. Geometry of the problem and coordinates system.

Mass conservation of the mixture in the channel along the flow direction thus yields

$$\frac{\partial(\rho u)}{\partial y} = \frac{M^{H_2} I}{2FL_x} \quad (1)$$

Here, ρ is the mixture density, M^{H_2} is the molecular weight of hydrogen, I is the current density, F is Faraday's constant and L_x is the channel dimension in the through-plane (X) direction. The source term stems from the mass of H_2 added to the cathode channel due to the production of H_2O (e.g., Wang et al., 2008). Integrating Eq. (1) in the flow direction and multiplying by channel cross section area ($A_{xz} \equiv L_x L_z$) we get

$$A_{xz} \rho u = A_{xz} (\rho u)_{in} + \frac{L_z M^{H_2}}{2F} \int_0^y I dy \quad (2)$$

where, L_z is the channel dimension in the in-plane direction (Z) and the subscript 'in' refers to inlet. Since

$$(\rho u)_{in} = \rho_g \zeta_c \frac{I_{avg} A_{mem}}{4FC_{in}^{O_2} A_{xz}} \quad (3)$$

where, ρ_g is the density of gas (air), ζ_c is the stoichiometry at cathode, I_{avg} is the average current density of the cell, A_{mem} is the cross sectional area of the membrane (or active area) and $C_{in}^{O_2}$ is the mole fraction of oxygen at inlet. Combining Eq. (2) and Eq. (3) we get

$$\rho u = \frac{I_{avg} A_{mem} M^{H_2}}{4FA_{xz}} \left[\frac{\rho_g}{C_{in}^{O_2} M^{H_2}} \zeta_c + 2 \int_0^y \frac{I}{I_{avg} L} dy \right] \quad (4)$$

For convenience, we define the following non-dimensional variables and numbers

$$Y = \frac{y}{L} \quad (5a)$$

$$\bar{I} = \frac{I}{I_{avg}} \quad (5b)$$

$$\psi = \frac{\rho_g}{C_{in}^{O_2} M^{H_2}} \quad (5c)$$

The inlet flux required at that operating condition is defined as the following:

$$\zeta = \frac{I_{avg} A_{mem} M^{H_2}}{4FA_{xz}} \quad (5d)$$

With the above definition of dimensionless variables/numbers, $2/\psi$ represents fractional increase in density if all the oxygen produces water and all of the product water is carried into the cathode channel whereas 2ζ represents the mass flux of hydrogen into the cathode channel due to water production. Moreover, we can reduce Eq. (4) to a compact form as follows:

$$\rho u = \zeta \left[\psi \zeta_c + 2 \int_0^Y \bar{I} dY \right] \quad (6)$$

which can be simplified further by introducing the following two additional assumptions:

- (4) Current production is taken to be independent of axial location y (cf. St-Pierre et al., 2008) that is,

$$I = \text{Const.}$$

- (5) When the stoichiometry of oxygen is greater than or equal to unity, we take the current density to be I_{avg} (A/m^2). But when the stoichiometry is less than unity, we assume 100% oxygen utilization. Therefore, the current density

becomes $\zeta_c I_{avg}$ (A/m^2). So we have

$$\bar{I}(\zeta_c, Y) = 1.0 \quad \text{for } \zeta_c \geq 1.0$$

$$\bar{I}(\zeta_c, Y) = \zeta_c \quad \text{for } \zeta_c < 1.0$$

Applying these assumptions to Eq. (6), we get

$$\rho u(\zeta_c, Y) = \zeta [\psi \zeta_c + 2Y] \quad \text{for } \zeta_c \geq 1.0 \quad (7a)$$

$$\rho u(\zeta_c, Y) = \zeta \zeta_c [\psi + 2Y] \quad \text{for } \zeta_c < 1.0 \quad (7b)$$

- (6) The gas channel is assumed to be isothermal. Although temperature variation along the channel is an important practical effect (Wilkinson and St-Pierre, 2003), it is not included. Since electrochemistry is not solved here, temperature variation can only be an external input at the boundary. Major portion of the waste heat generated in a PEFC is transported out by conduction through bipolar plates. High conductivity of bipolar plates usually keeps the temperature variation along the stream-wise direction within a few °C. Therefore, isothermal assumption is justified for a simplified analysis.

The phase mobility of liquid and gas phases are defined with respect to their relative permeability and kinematic viscosity as the following (Wang and Cheng, 1996):

$$\lambda_l = \frac{k_{rl}/\nu_l}{k_{rl}/\nu_l + k_{rg}/\nu_g} \quad \text{and} \quad \lambda_g = 1 - \lambda_l \quad (8)$$

where ν is the kinematic viscosity, k_{rl} and k_{rg} are the relative permeability of liquid phase and gas phase, respectively. The relative permeabilities are usually taken as exponential functions of liquid volume fraction 's'. This function could be determined by empirical curve fitting (Dullien, 1992). Here the functions are taken as, $k_{rl} = s^5$ and $k_{rg} = (1-s)^5$ (cf., Wang et al., 2008, Basu et al., 2009). Using the continuity equation and the species conservation equation, we obtain (Wang et al., 2008)

$$\lambda_l = \frac{\frac{\zeta_c}{2} \left(\frac{C^{H_2O}}{C^{O_2}} \right)_{in} + \frac{\int_0^y I dy}{I_{avg} L} - \frac{C_{sat}^{H_2O}}{\rho_g} \left(\frac{\zeta_c}{2} \left(\frac{\rho}{C^{O_2}} \right)_{in} + \frac{\int_0^y I dy}{I_{avg} L} M^{H_2} \right)}{\left(\frac{1}{M^{H_2O}} - \frac{C_{sat}^{H_2O}}{\rho_g} \right) \left(\frac{\zeta_c}{2} \left(\frac{\rho}{C^{O_2}} \right)_{in} + \frac{\int_0^y I dy}{I_{avg} L} M^{H_2} \right)} \quad \text{and} \quad \lambda_l \geq 0 \quad (9)$$

Using assumptions 4 and 5, we can simplify Eq. (9) as follows:

$$\lambda_l = \frac{\frac{\zeta_c}{2} \left(\frac{C^{H_2O}}{C^{O_2}} \right)_{in} + Y - \frac{C_{sat}^{H_2O}}{\rho_g} \left(\frac{\zeta_c}{2} \left(\frac{\rho}{C^{O_2}} \right)_{in} + Y M^{H_2} \right)}{\left(\frac{1}{M^{H_2O}} - \frac{C_{sat}^{H_2O}}{\rho_g} \right) \left(\frac{\zeta_c}{2} \left(\frac{\rho}{C^{O_2}} \right)_{in} + Y M^{H_2} \right)} \quad \text{for } \zeta_c \geq 1.0$$

$$\lambda_l = \frac{\frac{\zeta_c}{2} \left(\frac{C^{H_2O}}{C^{O_2}} \right)_{in} + \zeta_c Y - \frac{C_{sat}^{H_2O}}{\rho_g} \left(\frac{\zeta_c}{2} \left(\frac{\rho}{C^{O_2}} \right)_{in} + \zeta_c Y M^{H_2} \right)}{\left(\frac{1}{M^{H_2O}} - \frac{C_{sat}^{H_2O}}{\rho_g} \right) \left(\frac{\zeta_c}{2} \left(\frac{\rho}{C^{O_2}} \right)_{in} + \zeta_c Y M^{H_2} \right)} \quad \text{for } \zeta_c < 1.0$$

and $\lambda_l \geq 0$ (10)

By defining the following two non-dimensional parameters:

$$\alpha = \frac{\frac{1}{M^{H_2}} - \frac{C_{sat}^{H_2O}}{\rho_g}}{\frac{1}{M^{H_2O}} - \frac{C_{sat}^{H_2O}}{\rho_g}} \quad (11a)$$

$$\beta = \frac{\frac{C_{sat}^{H_2O}}{2M^{H_2} C_{in}^{O_2}} - \frac{C_{sat}^{H_2O}}{\rho_g}}{\frac{1}{M^{H_2O}} - \frac{C_{sat}^{H_2O}}{\rho_g}} \quad (11b)$$

we can simplify Eq. (10) by regrouping as

$$\lambda_l = \alpha - \frac{\beta + \frac{\alpha\psi}{2}}{\frac{Y}{\xi_c} + \frac{\psi}{2}} \quad \text{for } \xi_c \geq 1.0$$

$$\lambda_l = \alpha - \frac{\beta + \frac{\alpha\psi}{2}}{Y + \frac{\psi}{2}} \quad \text{for } \xi_c < 1.0 \quad \text{and } \lambda_l \geq 0 \quad (12)$$

One can easily check Eq. (12), by substituting the variables defined in Eqs. (5) and (11).

In Eq. (11) β represents the capacity of the inlet flow to take up water in vapor form. Accordingly, for saturated flow at the inlet, β is zero.

For an unsaturated flow at the inlet ($\beta > 0$), the inlet is always dry. The liquid starts to appear when in Eq. (12)

$$\lambda_l = 0 \quad (13)$$

This gives

$$Y_{dry} = Y|_{\lambda_l=0} = \frac{\beta}{\alpha} \xi_c \quad \text{for } \xi_c \geq 1.0 \quad (14a)$$

$$Y_{dry} = Y|_{\lambda_l=0} = \frac{\beta}{\alpha} \quad \text{for } \xi_c < 1.0 \quad (14b)$$

This is subject to the constraint $Y_{dry} \leq 1.0$. From these equations we can see that for saturated flow at the inlet, two-phase flow also starts at the inlet. Moreover, as the stoichiometry increases, the dry length of the channel would increase linearly with it.

Using the definition of liquid mobility λ_l from Eq. (8) we have

$$s = \frac{1}{\left(\frac{1-\lambda_l}{\lambda_l} \left(\frac{v_g}{v_l}\right)\right)^{1/5} + 1} \quad \text{for } \lambda_l > 0$$

$$s = 0 \quad \text{for } \lambda_l = 0 \quad (15)$$

For steady-state, one-dimensional two-phase flow in the channels, the momentum equation (following Darcy Law) reduces to

$$\frac{\partial P}{\partial y} = -\frac{v}{K}(\rho u) \quad (16)$$

Therefore, we can compute the total pressure drop as follows:

$$\Delta P = -\int_0^L \left(\frac{\partial P}{\partial y}\right) dy \quad (17)$$

In Eq. (16), the permeability K is taken to be known and the flux can be computed as a function of Y from Eq. (7). The value of the mixture viscosity can be obtained using the following mixture rule (Wang and Cheng, 1996):

$$v = \left(\frac{k_{rl}}{v_l} + \frac{k_{rg}}{v_g}\right)^{-1} \quad (18)$$

Using Eq. (15) in the constitutive relation for the relative permeabilities, we get

$$k_{rl} = s^5 = \frac{\lambda_l v_l}{[(1-\lambda_l)v_g]^{1/5} + (\lambda_l v_l)^{1/5}]^5} \quad (19)$$

and

$$k_{rg} = (1-s)^5 = \frac{(1-\lambda_l)v_g}{[(1-\lambda_l)v_g]^{1/5} + (\lambda_l v_l)^{1/5}]^5} \quad (20)$$

Therefore, we get from Eq. (18)

$$v = [(1-\lambda_l)v_g]^{1/5} + (\lambda_l v_l)^{1/5}]^5 \quad (21)$$

Using Eqs. (19) and (20) in the pressure drop relation, Eq. (17), we have

$$\Delta P = \int_0^L \frac{v}{K}(\rho u) dy = \frac{1}{K} \int_0^L [(1-\lambda_l)v_g]^{1/5} + (\lambda_l v_l)^{1/5}]^5 (\rho u) dy \quad (22)$$

By defining the following non-dimensional mixture kinematic viscosity:

$$\bar{v} = \frac{v}{v_g} = [(1-\lambda_l)^{1/5} + (\lambda_l v_l/v_g)^{1/5}]^5 \quad (23)$$

We can simplify Eq. (22) to arrive at

$$\Delta P = \frac{v_g L}{K} \zeta \int_0^L \bar{v} [\psi \xi_c + 2Y] dY \quad \text{for } \xi_c \geq 1.0 \quad (24a)$$

$$\Delta P = \frac{v_g L}{K} \zeta \int_0^L \bar{v} \xi_c [\psi + 2Y] dY \quad \text{for } \xi_c < 1.0 \quad (24b)$$

In the integral in Eq. (22), the term (ρu) is a linear function of y , while the mixture viscosity is not an integrable function. However, for a single-phase flow Eq. (22) is integrable as $\bar{v} = 1.0$ (here, \bar{v} is the non-dimensional mixture kinematic viscosity as defined in Eq. (23)).

For all parallel gas channels, the pressure drop for each channel should remain equal. Due to GDL intrusion into the channels, the cross-section area of the channel decreases. This would mean less flow in that channel; and therefore, the local stoichiometry would decrease. To keep the average stoichiometry the same, velocity would increase in the unintruded channels. Therefore, the pressure drop would increase. The GDL intrusion is considered only at the end channels of the parallel channels. If the number of parallel channels (i.e. 'n') is large, then we can neglect the increment of the flow velocity in the unintruded channels. Let δ be the fractional reduction in cross-section area of the channel and ε the fractional reduction in local stoichiometry (or dimensionless flowrate). Consequently, we have the following:

For an intruded channel,

$$A_{xz} = \bar{A}_{xz}(1-\delta)$$

$$\xi_c = \bar{\xi}_c(1-\varepsilon) \quad (25)$$

The permeability of the intruded channel also decreases due to GDL intrusion. Using the Hagen–Poiseuille equation we get (cf., Wang et al., 1994)

$$K = c \frac{d_h^2}{32} \quad (26)$$

Since

$$d_h = 4 \frac{L_x \frac{L_z}{2}}{2(L_x + \frac{L_z}{2})},$$

Eq. (26) becomes upon substitution

$$K = \frac{c}{8} \left(\frac{L_x \frac{L_z}{2}}{L_x + \frac{L_z}{2}} \right)^2 \quad (27)$$

Due to GDL intrusion, length in the x-direction decreases. Thus, for the intruded channel we get

$$K = \frac{c}{8} \left(\frac{L_z}{2} \right)^2 \frac{(1-\delta)^2}{\left((1-\delta) + \frac{L_z/2}{L_x} \right)^2} \quad (28)$$

In the present work, we assume $L_z/2/L_x = 2.0$. Therefore, we can approximate the expression for channel permeability as

$$K = \frac{c}{8} \left(\frac{L_x \frac{L_z}{2}}{L_x + \frac{L_z}{2}} \right)^2 (1-\delta)^2 = \bar{K}(1-\delta)^2 \quad (29)$$

where \bar{K} is the channel permeability without GDL intrusion. We have computed the exact value of channel permeability as a function of δ using a CFD (computational fluid dynamics) code. The numerically computed K is compared to the approximate estimate expressed by Eq. (29) as shown in Fig. 3. It is clear that our simple approximate formula can closely approximate the exact relation between channel permeability and GDL intrusion.

For an unintruded channel

$$\begin{aligned} A_{xz} &= \bar{A}_{xz} \\ K &= \bar{K} \\ \xi_c &= \bar{\xi}_c \left(1 + \frac{2}{n-2} \varepsilon \right) \end{aligned} \quad (30)$$

where n is the number of parallel channels. So, for a parallel network of channels we have,

$$\Delta P = \Delta P(\bar{\xi}_c, \delta, \varepsilon)_{intruded} = \Delta P(\bar{\xi}_c, \delta, \varepsilon)_{unintruded} \quad (31)$$

Using Eqs. (25) and (29) on Eq. (24) we have

$$\frac{\Delta P_{intruded}}{\frac{v_e L}{K} \zeta} = \frac{1}{(1-\delta)^3} \int_0^1 \bar{v}(\bar{\xi}_c(1-\varepsilon), Y) [\psi \bar{\xi}_c(1-\varepsilon) + 2Y] dY \quad (32a)$$

for $\bar{\xi}_c(1-\varepsilon) \geq 1.0$

$$\frac{\Delta P_{intruded}}{\frac{v_e L}{K} \zeta} = \frac{1}{(1-\delta)^3} \int_0^1 \bar{v}(\bar{\xi}_c(1-\varepsilon), Y) \bar{\xi}_c(1-\varepsilon) [\psi + 2Y] dY \quad (32b)$$

for $\bar{\xi}_c(1-\varepsilon) < 1.0$

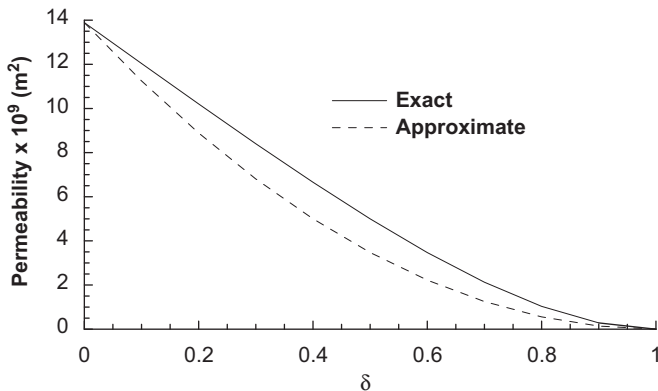


Fig. 3. Exact and approximate solutions of flow permeability as a function of GDL intrusion.

Using Eq. (30) on Eq. (24), we get

$$\frac{\Delta P_{unintruded}}{\frac{v_e L}{K} \zeta} = \int_0^1 \bar{v} \left(\bar{\xi}_c \left(1 + \frac{2}{n-2} \varepsilon \right), Y \right) \left[\psi \bar{\xi}_c \left(1 + \frac{2}{n-2} \varepsilon \right) + 2Y \right] dY \quad (33)$$

Now we can combine Eqs. (32) and (33) to find a relation between area maldistribution (δ) and flow maldistribution (ε)

$$\delta = 1 - \left[\frac{\int_0^1 \bar{v}(\bar{\xi}_c(1-\varepsilon), Y) [\psi \bar{\xi}_c(1-\varepsilon) + 2Y] dY}{\int_0^1 \bar{v} \left(\bar{\xi}_c \left(1 + \frac{2}{n-2} \varepsilon \right), Y \right) \left[\psi \bar{\xi}_c \left(1 + \frac{2}{n-2} \varepsilon \right) + 2Y \right] dY} \right]^{1/3} \quad (34a)$$

for $\bar{\xi}_c(1-\varepsilon) \geq 1.0$

$$\delta = 1 - \left[\frac{\int_0^1 \bar{v}(\bar{\xi}_c(1-\varepsilon), Y) \bar{\xi}_c(1-\varepsilon) [\psi + 2Y] dY}{\int_0^1 \bar{v} \left(\bar{\xi}_c \left(1 + \frac{2}{n-2} \varepsilon \right), Y \right) \left[\psi \bar{\xi}_c \left(1 + \frac{2}{n-2} \varepsilon \right) + 2Y \right] dY} \right]^{1/3} \quad (34b)$$

for $\bar{\xi}_c(1-\varepsilon) < 1.0$

In the case of single-phase flow we have $\bar{v} = 1.0$ and thus Eq. (34) can be integrated. Therefore, for single phase flow we have

$$\delta = 1 - \left[\frac{\psi \bar{\xi}_c(1-\varepsilon) + 1}{\psi \bar{\xi}_c \left(1 + \frac{2}{n-2} \varepsilon \right) + 1} \right]^{1/3} \quad \text{for } \bar{\xi}_c(1-\varepsilon) \geq 1.0 \quad (35a)$$

$$\delta = 1 - \left[\bar{\xi}_c(1-\varepsilon) \frac{\psi + 1}{\psi \bar{\xi}_c \left(1 + \frac{2}{n-2} \varepsilon \right) + 1} \right]^{1/3} \quad \text{for } \bar{\xi}_c(1-\varepsilon) < 1.0 \quad (35b)$$

With these sets of equations, it is possible to develop a map of area maldistribution vs. flow maldistribution, which can provide a range of parameters for safe operation and the minimum or stoichiometric amount of oxygen reactant that needs to be supplied to all channels.

Since, the value of ψ is of the order of 70 we can neglect $2Y$ with respect to it. Implementing this approximation in Eq. (34) we can get

$$\frac{\int_0^1 \bar{v}(\bar{\xi}_c(1-\varepsilon), Y) dY}{\int_0^1 \bar{v} \left(\bar{\xi}_c \left(1 + \frac{2}{n-2} \varepsilon \right), Y \right) dY} = (1-\delta)^3 \frac{1 + \frac{2\varepsilon}{n-2}}{1-\varepsilon} \quad (36)$$

Let us define average kinematic viscosity for a channel as the following:

$$\tilde{v} = \int_0^1 \bar{v} dY = Y_{dry} + \int_{Y_{dry}}^1 \bar{v} dY \quad (37)$$

The first term of the right hand side of Eq. (37) is due to the dry part of the channel (single-phase flow) and the second term is due to the wet part of the channel (two-phase flow). Mixture kinematic viscosity is greater than the kinematic viscosity of air ($\bar{v} > 1.0$). Therefore, \tilde{v} is a decreasing function of Y_{dry} . Using Eq. (37) on the left hand side of Eq. (36) of we can get

$$\begin{aligned} \frac{\tilde{v}_{intruded}}{\tilde{v}_{unintruded}} &= \frac{\int_0^1 \bar{v}(\bar{\xi}_c(1-\varepsilon), Y) dY}{\int_0^1 \bar{v} \left(\bar{\xi}_c \left(1 + \frac{2}{n-2} \varepsilon \right), Y \right) dY} \\ &= \frac{Y_{dry}^{intruded} + \int_{Y_{dry}^{intruded}}^1 \bar{v}(\bar{\xi}_c(1-\varepsilon), Y) dY}{Y_{dry}^{unintruded} + \int_{Y_{dry}^{unintruded}}^1 \bar{v} \left(\bar{\xi}_c \left(1 + \frac{2}{n-2} \varepsilon \right), Y \right) dY} \end{aligned} \quad (38)$$

Total number of parallel channels (n) are usually large for most of the designs. So, the dependence of $\tilde{v}_{unintruded}$ on flow

maldistribution ε is weak. Hence, the denominator of Eq. (38) could be taken as constant for a given operating condition. Using that we can rearrange Eq. (38) as

$$\frac{\tilde{v}_{intruded}}{\tilde{v}_{unintruded}} = \frac{(Y_{dry}^{unintruded} - \Delta Y_{dry}) + \int_{Y_{dry}^{unintruded} - \Delta Y_{dry}}^1 \bar{v}(\bar{\xi}_c(1-\varepsilon), Y) dY}{Y_{dry}^{unintruded} + \int_{Y_{dry}^{unintruded}}^1 \bar{v}(\bar{\xi}_c(1 + \frac{2}{n-2}\varepsilon), Y) dY} \quad (39)$$

where $\Delta Y_{dry} (= Y_{dry}^{unintruded} - Y_{dry}^{intruded})$.

The difference in dry length between intruded and unintruded channels is important because flow resistance in two-phase flow is several times the flow resistance in single-phase flow. Therefore, as the ΔY_{dry} increases the flow resistance in the intruded channel (with respect to the unintruded channel) also increases. For a parallel channel configuration, the total pressure drop is the same for both the intruded and the unintruded channel. Therefore, if the flow resistance is large in the intruded channel, even a small GDL intrusion will result in appreciable flow maldistribution. This would decrease a PEFC's ability to tolerate GDL intrusion. The dry length of a channel can be determined using Eq. (14). The difference of dry length ΔY_{dry} between the intruded and unintruded channel is

$$\begin{aligned} \Delta Y_{dry} &= Y_{dry}^{unintruded} - Y_{dry}^{intruded} = \frac{\beta}{\alpha} \bar{\xi}_c \varepsilon \frac{n}{n-2} \\ \text{for } \frac{\beta}{\alpha} \bar{\xi}_c \left(1 + \frac{2}{n-2}\varepsilon\right) &\leq 1.0 \\ \Delta Y_{dry} &= 1 - \frac{\beta}{\alpha} \bar{\xi}_c (1-\varepsilon) \\ \text{for } \frac{\beta}{\alpha} \bar{\xi}_c \left(1 + \frac{2}{n-2}\varepsilon\right) &> 1.0 > \frac{\beta}{\alpha} \bar{\xi}_c (1-\varepsilon) \\ \Delta Y_{dry} &= 0 \quad \text{for } \frac{\beta}{\alpha} \bar{\xi}_c (1-\varepsilon) \geq 1.0 \end{aligned} \quad (40)$$

As ΔY_{dry} increases, the first term in the right hand side numerator of Eq. (39) decreases, while the second term increases. Since $\bar{v} > 1.0$ for the operational range, $\tilde{v}_{intruded}/\tilde{v}_{unintruded}$ is an increasing function of ΔY_{dry} . From the design perspective for smooth operation of a PEFC, a certain allowable flow maldistribution can be fixed. Combining Eqs. (36) and (39) we get

$$\begin{aligned} \frac{\tilde{v}_{intruded}}{\tilde{v}_{unintruded}} &= \frac{(Y_{dry}^{unintruded} - \Delta Y_{dry}) + \int_{Y_{dry}^{unintruded} - \Delta Y_{dry}}^1 \bar{v}(\bar{\xi}_c(1-\varepsilon), Y) dY}{Y_{dry}^{unintruded} + \int_{Y_{dry}^{unintruded}}^1 \bar{v}(\bar{\xi}_c(1 + \frac{2}{n-2}\varepsilon), Y) dY} \\ &= (1-\delta)^3 \frac{1 + \frac{2\varepsilon}{n-2}}{1-\varepsilon} \end{aligned} \quad (41)$$

Therefore, from Eq. (41) we can see that given the allowable flow maldistribution (ε), the greater $\tilde{v}_{intruded}/\tilde{v}_{unintruded}$, the smaller allowable GDL intrusion (δ) is. This indicates that with increasing ΔY_{dry} , allowable GDL intrusion δ decreases. Thus, we can consider that ΔY_{dry} is the parameter that controls maldistribution. For an optimal design, ΔY_{dry} has to be minimized.

3. Results and discussion

Although, experimental validation is essential for any model, suitable data are not always available. In our case, obtaining such a data is a challenge and to the best of the authors' knowledge no such investigation exists in literature. Thus, we validated the liquid volume fraction results against the three-dimensional CFD model and calibrated the model for pressure drop along the channel (Wang et al., 2008). Effect of net water transport coefficient could be included into the model using external input.

It is also possible to add spatial variation to this. Variation in net water transport coefficient could result in drastic change in pressure drop and liquid volume fraction distribution. Despite some available data (Wilkinson and St-Pierre, 2003), this effect is kept for further investigation when more specific data experimental data will become available.

To demonstrate the utility of our analytical model, we choose a PEFC configuration with seven parallel channels with the end channels being prone to GDL intrusion. Since low stoichiometry operation minimizes the parasitic power loss, a stoichiometry of 2.0 is used in the present work. Using Eqs. (34) and (35), we can estimate the extent of GDL intrusion for a given maldistribution in terms of stoichiometry. The cell operating temperature is taken as 80°C where the inlet relative humidity is taken as 67%. This condition means the inlet has no liquid water and cathode flow can carry some water in vapor form, resulting in low pressure drop in the gas channel. Some investigations (cf. Knights et al., 2004) have suggested low performance in the case of dry inlet condition. In practice, a compromise is reached generally between 60% and 80% relative humidity. However, a sensitivity analysis has been performed for inlet relative humidity variation.

It is clear from Fig. 4 that in single-phase flow the extent of flow maldistribution is always much severe than the extent of areal maldistribution. This effect is even more pronounced for two-phase flow as shown in Fig. 4. Also plotted in Fig. 4 is the $\varepsilon = \delta$ curve to help the reader visualize how much the flow maldistribution is greater than the area maldistribution. In the present case, $\varepsilon > 0.5$ would make the local stoichiometry in the intruded channels less than unity. This condition is undesirable for stable PEFC operations. From Fig. 4, we can see that this condition may occur for an area maldistribution as low as 0.2.

Liquid volume fraction in the stream-wise direction of the channel could be calculated by substituting Eqs. (12) and (13) in Eq. (15). When flow maldistribution (ε) is equal to 0.1, there is a visible difference in the liquid saturation profile as shown in Fig. 5. The same conditions are simulated using the three-dimensional M2 model (Basu et al., 2009, Wang et al., 2008) to verify this model's predictions. In Fig. 5, the lines represent analytical model predictions whereas symbols denote the 3-D model predictions. The results of three-dimensional simulation

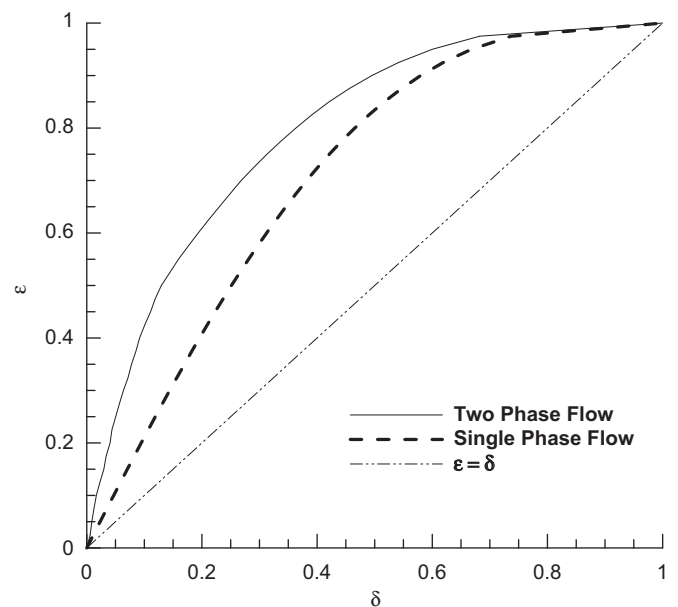


Fig. 4. Relationship between flow maldistribution and GDL intrusion factor (or cross-sectional area difference) ($\bar{\xi}_c = 2.0$, RH=67%).

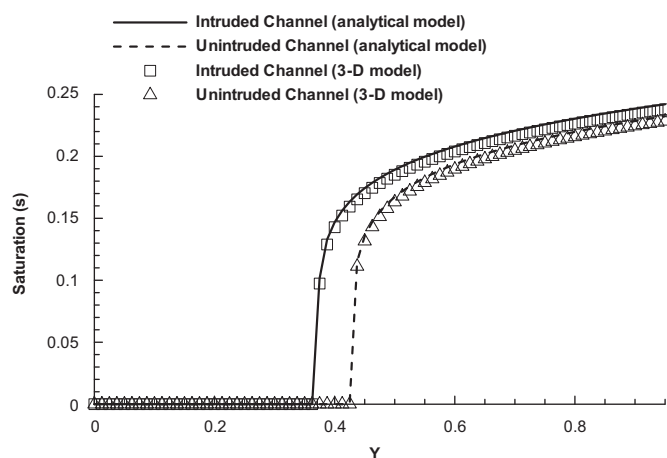


Fig. 5. Liquid saturation profiles in intruded and unintruded channels for $\varepsilon = 0.1$ ($\bar{\zeta}_c = 2.0$, RH=67%), analytical and 3-D simulation results.

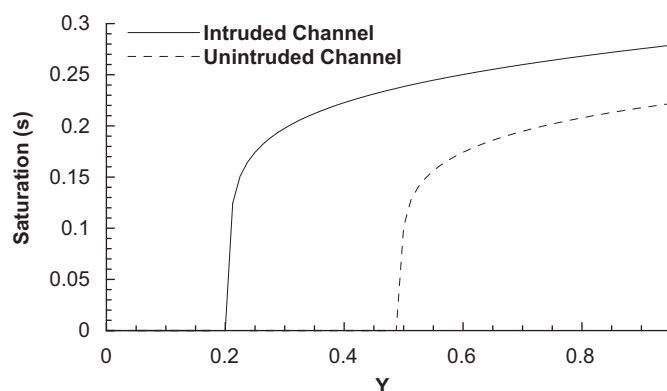


Fig. 6. Liquid saturation profiles in intruded and unintruded channels for $\varepsilon = 0.5$ ($\bar{\zeta}_c = 2.0$, RH=67%).

and the present analytical model differ by about 1%. Dry length decreases in the intruded channel due to low flow rate. Moreover, the maximum liquid saturation increases in the intruded channels.

As flow maldistribution (ε) is increased to 0.5, difference in the liquid saturation profile is enormous as displayed in Fig. 6. Notably, the flow situation in the perfect channel does not change much. But the dry length decreases in the intruded channel and amount of liquid at exit is much higher. When flow maldistribution is 0.5, the local stoichiometry reaches unity. So at higher flow maldistribution than this, the liquid saturation in the intruded channel no longer depends on the local stoichiometry (Eq. (12)) due to low current production. This effect is shown in Fig. 7, for flow maldistribution of 0.9.

Comparing Figs. 6 and 7, we can see that the saturation distributions in the intruded channels are the same in both cases. This is due to the reason pointed out earlier. But the higher flow maldistribution causes more flow in the perfect channel. Consequently, the dry length in the perfect channel increases but the overall liquid saturation decreases.

3.1. Mitigating flow maldistribution

A typical distribution of dry channel length between intruded and unintruded channels is schematically shown in Fig. 8. The amount of GDL intrusion depends on the fabrication or assembling pressure and the GDL material. For a better material, which results in lesser intrusion, it is easier to keep the flow

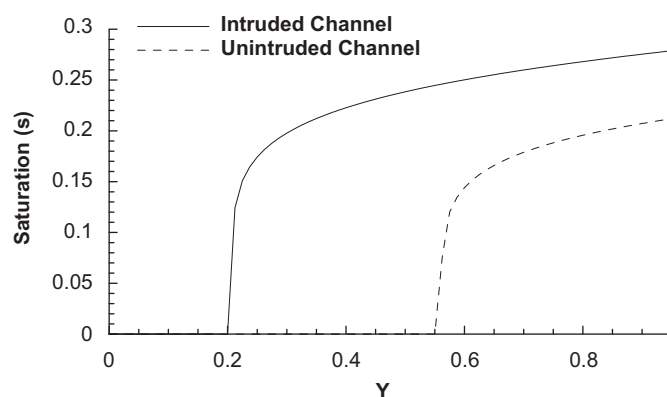


Fig. 7. Liquid saturation profiles in intruded and unintruded channels for $\varepsilon = 0.9$ ($\bar{\zeta}_c = 2.0$, RH=67%).

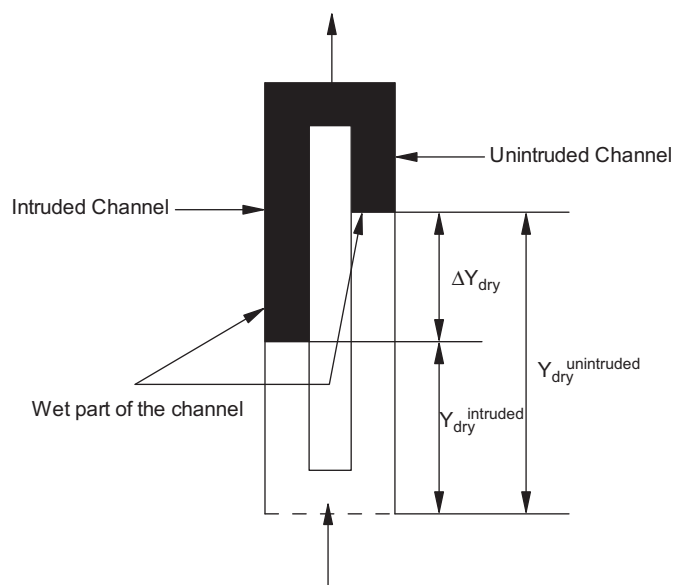


Fig. 8. Schematic of dry length in parallel flowfield with one intruded and one unintruded channel.

maldistribution within the required range. It is also possible to tweak other parameters to keep the flow maldistribution within the required range. We have already seen that two-phase flow exacerbates flow maldistribution. The ability of flow in channels to transport water in form of vapor increases when the inlet RH is reduced. In the set of governing equations presented in this work, the RH reduction is reflected in the increment in β .

From Eq. (40), it is clear that for a specified geometry and a fixed flow maldistribution, parameters controlling ΔY_{dry} are β (measure of dryness of flow at the inlet or inflow) and global stoichiometry $\bar{\zeta}_c$. Difference in dry length (ΔY_{dry}) increases linearly with β and $\bar{\zeta}_c$ till the unintruded channel becomes completely dry. Then, it decreases linearly with β and $\bar{\zeta}_c$, till the intruded channel becomes completely dry, resulting in $\Delta Y_{dry} = 0$. After this, both the channel becomes completely dry and ΔY_{dry} remains equal to zero. At this point the allowable GDL intrusion becomes equal to the allowable GDL intrusion for single-phase flow. Note here that, the non-dimensional group $(\beta/\alpha)\bar{\zeta}_c$ is defined as a measure of the inlet condition to keep the flow dry. For convenience, we define

$$\eta(T_{in}, \bar{\zeta}_c) = \frac{\beta}{\alpha} \bar{\zeta}_c \quad (42)$$

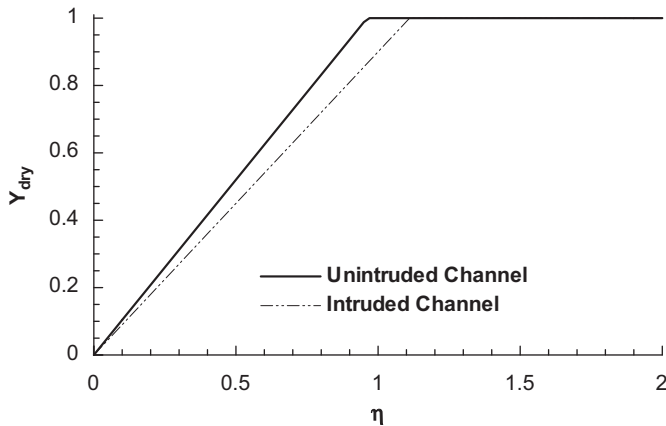


Fig. 9. Variation of dry length for intruded and unintruded channels for flow maldistribution.

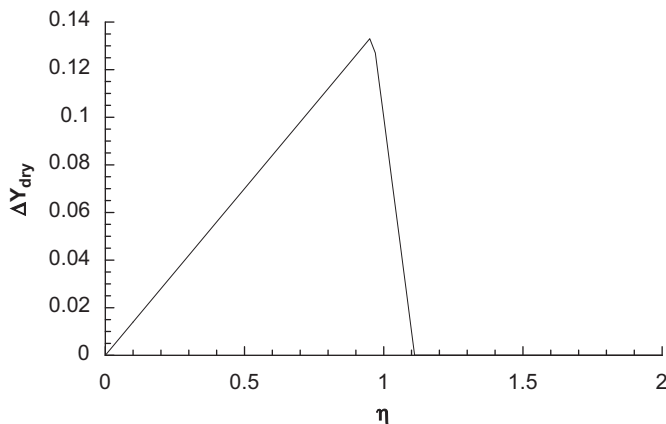


Fig. 10. Difference in the dry length between intruded and unintruded channels at flow maldistribution $\varepsilon=0.1$.

Physically, $Y_{dry} \leq 1.0$, but η represents the dry length were the channel infinitely long. Keeping the flow maldistribution (ε) at 0.1, the dry lengths in intruded and unintruded channels are computed for varying η and the results are plotted in Fig. 9. The difference between the dry lengths of intruded and unintruded channels (ΔY_{dry}) is plotted against η in Fig. 10. This difference is zero for fully humidified flow ($\eta=0.0$) but it increases with increasing η for the system. This η can be increased by raising the stoichiometry or lowering the relative humidity. This trend continues till the unintruded channel becomes completely dry; in other words, the dry length in the unintruded channel becomes constant and equal to unity. If η is increased further, difference between dry length decreases rapidly till the intruded channel becomes dry also. At this point, ΔY_{dry} becomes zero again and increasing η further has no effect on ΔY_{dry} . Again, from Eq. (40), we can see that it is possible to minimize ΔY_{dry} by increasing RH or decreasing stoichiometry if the unintruded channel remains wet. When the unintruded channel is dry, ΔY_{dry} can be reduced by either decreasing the relative humidity or by increasing the stoichiometry. If both intruded and unintruded channels are dry, ΔY_{dry} is zero and thus the lowest possible maldistribution is achieved.

3.2. Effect of global stoichiometry

The global stoichiometry has a profound effect on the flow maldistribution for a given GDL intrusion. By examining Eqs. (34)

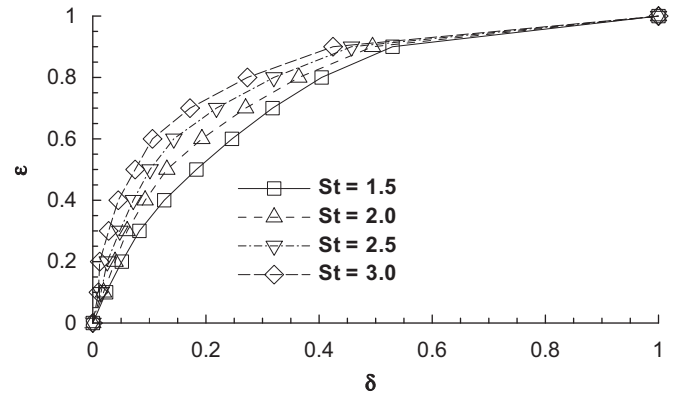


Fig. 11. Effect of average flow stoichiometry on maldistribution for inlet RH=67%.

and (35), we can see that the difference in local stoichiometry is greater at larger global stoichiometry. Therefore, the same amount of GDL intrusion results in greater flow maldistribution as the global stoichiometry increases. In Fig. 11, flow maldistribution is plotted against area maldistribution for various global stoichiometries. It is generally believed that using higher stoichiometry, it is possible to mitigate flow maldistribution by using higher global stoichiometry. From the analysis presented earlier, we show that for a fixed flow maldistribution, GDL intrusion decreases as ΔY_{dry} increases. In the present case, for stoichiometry of 2.0, the unintruded channel never gets completely dry. Therefore, we remain confined in the first part of Fig. 10, in which increasing stoichiometry or decreasing RH exacerbates the maldistribution situation.

We can predict the effect of global stoichiometry on smooth PEFC operation from Fig. 11. Let us consider that the minimum allowable stoichiometry in every channel for smooth operation of the cell is unity. At a global stoichiometry of 1.5, local stoichiometry in the intruded channels reach unity for a GDL intrusion of 0.11. This value of GDL intrusion is termed as allowable GDL intrusion. As we increase the global stoichiometry, the allowable GDL intrusion also increases. At the global stoichiometry of 2.0, the allowable GDL intrusion is 0.17. When we increase the global stoichiometry to 3.0, the allowable GDL intrusion is 0.20. This indicates that allowable GDL intrusion does not increase appreciably even if the global saturation is raised by 50%.

3.3. Effect of relative humidity

In Fig. 12, the flow maldistribution is plotted against GDL intrusion for various values of inlet relative humidity. The average stoichiometry is set at 2.0 for all cases. For a given flow maldistribution, we require as much allowable GDL maldistribution as possible for a good design. From Fig. 12, it is clear that when the relative humidity is low, the allowable GDL intrusion decreases more rapidly as compared with that when RH is high—this trend is predicted by our earlier analysis. Whereas the maximum allowable intrusion occurs for single-phase flow, the closest to that situation can be achieved using 100% RH at the inlet. But this will increase the pressure drop, and thus cause the parasitic pressure loss to rise. A trade-off between these can be found, depending on operating conditions and allowable parasitic loss and tolerable GDL intrusion. If allowable loss of flow in the intruded channels for a stoichiometry of 2.0 is set at 10%, our computed results show that the maximum allowable GDL intrusion is 4.67% for the single-phase flow. For fully humidified flow, the maximum allowable GDL intrusion is 3.9%. When the relative humidity is decreased to 67% (dew point

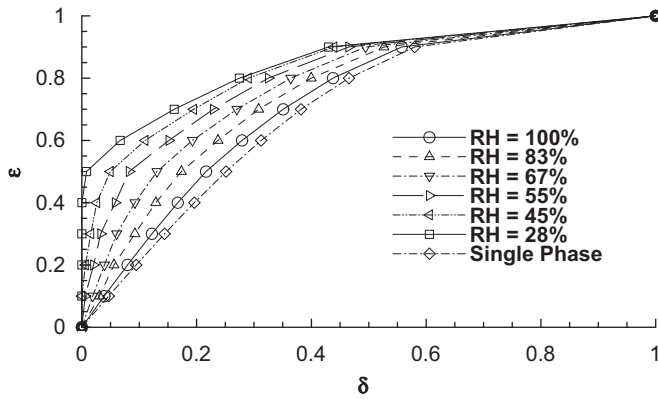


Fig. 12. Effect of inlet gas relative humidity on flow maldistribution for average flow stoichiometry $\bar{\zeta}_c = 2.0$.

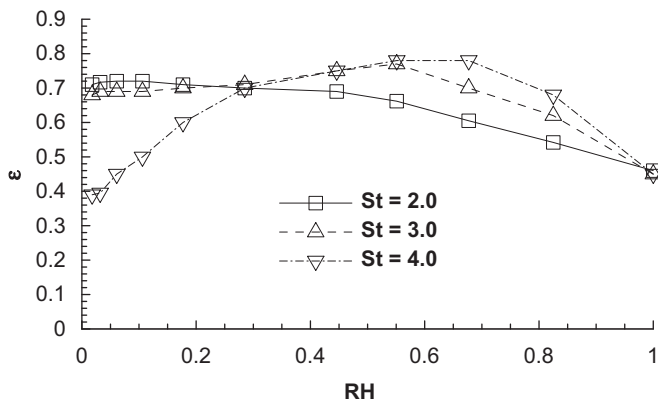


Fig. 13. Effect of inlet gas relative humidity on flow maldistribution for $\delta = 0.2$.

temperature 70°C), the maximum tolerable GDL intrusion decreases to 1.9%. For a relative humidity of 45% (dew point temperature 60°C), this tolerable GDL intrusion decreases to 0.1%. Therefore, in order to minimize flow maldistribution it is a good idea to keep reactant flow close to fully humidified.

In Fig. 13, flow maldistribution is plotted against relative humidity in which the GDL intrusion is fixed at 0.2 and the stoichiometry ranges from 2 to 4. At the stoichiometry of 2.0, the unintruded channel is always wet; therefore, decreasing the relative humidity results in increased flow maldistribution. At the stoichiometry of 3.0, when the relative humidity is decreased, the unintruded channel eventually becomes dry at RH=40%. Decreasing the RH beyond that has a favorable effect on flow maldistribution. At a high stoichiometry of 4.0, even the intruded channel becomes almost dry; therefore, the flow maldistribution at very low RH (~3%) is equal to that of the single-phase flow maldistribution.

3.4. Effect of flow-field design on minimizing GDL intrusion effects

GDL intrusion in the channels is inevitable till new materials with suitable properties can be developed. Accordingly, a flow-field design that can minimize the effect of GDL intrusion has to be identified. Since the GDL intrusion occurs at the channels that form the perimeter, for a fixed active area the perimeter of the flow field needs to be minimized. As an illustration, let's consider a serpentine flow field with n_t turns and n_c parallel channels, and the maximum length of the channel before first turn to be L in mm while the active area is A in mm^2 (as described in Fig. 14).

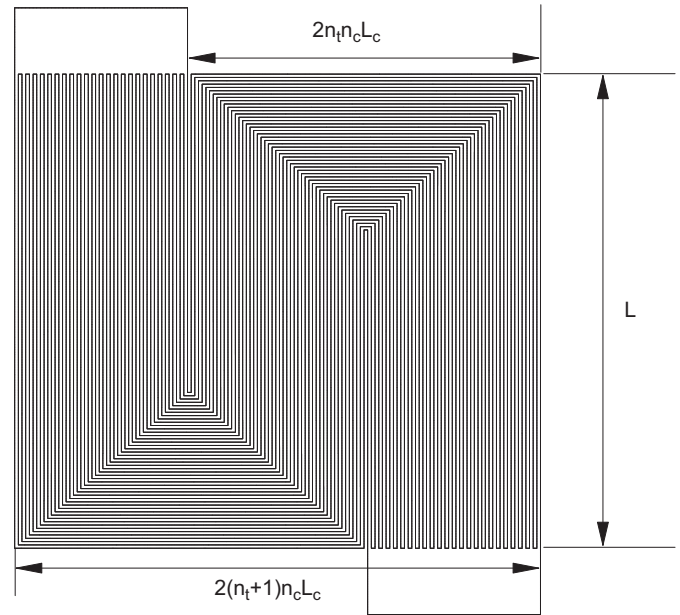


Fig. 14. Schematic of a serpentine flowfield and design parameters.

Moreover, let's assume that both land and channel widths are equal to L_c (mm). From these the area could be represented as

$$2(n_t + 1)n_c L_c L = A \quad (43)$$

For this configuration, the GDL intrusion occurs at the length is given by

$$L_{\text{gdl-intrusion}} = 2(2n_t n_c L_c + L) = 2 \left(2n_t n_c L_c + \frac{A}{2(n_t + 1)n_c L_c} \right) \quad (44)$$

From Eq. (44), we obtain the following optimal number of turns for a constant number of channels

$$n_t = \left(\frac{A}{4n_c^2 L_c^2} \right)^{1/2} - 1 \quad (45)$$

Along the same line, for a constant number of turns, the optimal number of channels is given by

$$n_c = \left(\frac{A}{4n_t(n_t + 1)L_c^2} \right)^{1/2} \quad (46)$$

From Eqs. (45) and (46), it is possible to easily compute the optimal flow-field geometry for a PEFC that is the most resistant to the GDL intrusion. For an industrial size PEFC, the optimal shape of the active area is a square as it has the least perimeter to area ratio of all rectangular shapes.

4. Conclusions

GDL intrusion in the flow channels of a PEFC can pose a serious problem to its smooth operation and thus threaten its stable performance. An analytical model, based on mass and momentum conservation in two-phase flow, was developed to elucidate effects of the GDL intrusion in the end channels on flow maldistribution in the channels. Results computed from our analytical model show that flow maldistribution is always more severe in a two-phase flow than in a single-phase flow. Our model is capable of predicting pressure, velocity and liquid saturation along the channel. Given a flow maldistribution, the difference in

liquid saturation distribution can be computed from our model. It is further indicated that dry length decreases in the intruded channel whereas the overall liquid volume fraction increases. For stable PEFC operation, a minimum stoichiometric supply of reactant should be maintained. At higher flow maldistribution, when the reactant flow in the intruded channels is less than one stoichiometry, saturation distribution in the intruded channels become independent of flow maldistribution.

It is found that the differential dry-length (ΔY_{dry}) is a key parameter controlling flow maldistribution. For a fixed flow maldistribution, lowering ΔY_{dry} can ensure higher tolerable GDL intrusion. Another finding is that when both intruded and unintruded channels are wet; increasing stoichiometry or decreasing relative humidity worsens flow maldistribution. When the unintruded channel is dry, these actions produce favorable outcome: that is, reducing flow maldistribution. When both intruded and unintruded channels are dry, tolerable GDL intrusion achieves its maximum. Hereafter, it becomes independent of stoichiometry and relative humidity. Our analysis further suggests that the effect of maldistribution is the least when the fully humidified inlet condition is used. Although channels remain drier in partially humidified conditions, the presence of liquid water varies widely between intruded and unintruded channels. This exacerbates the flow maldistribution and results in a very low allowable GDL intrusion for a given flow maldistribution. Lastly, as GDL intrusion is inevitable to a PEFC, a flow-field design inherently resistant to intrusion should be used. The optimal number of channels and turns for a desirable PEFC design are obtained by exercising our analytical model.

Acknowledgments

This work was funded by Sandia National Laboratories. Sandia is a multiprogram laboratory operated by Sandia Corporation, a Lockheed Martin Company, for the United States Department of Energy's National Nuclear Security Administration under contract DE-AC04-94AL85000.

References

- Anderson, R., Zhang, L., Ding, Y., Blanco, M., Bi, X., Wilkinson, D.P., 2010. A critical review of two-phase flow in gas flow channels of proton exchange membrane fuel cells. *J. Power Sour.* 195 (15), 4531–4533.
- Barrears, F., Lozano, A., Valiano, A., Marin, C., Pascau, A., 2005. Flow distribution in a bipolar plate of a proton exchange membrane fuel cell: experiments and numerical simulation studies. *J. Power Sour.* 144 (1), 54–66.
- Basu, S., Wang, C.Y., Chen, K.S., 2009. Two-phase flow maldistribution and mitigation in the cathode channels of a polymer electrolyte fuel cell. *Trans. ASME J. Fuel Cell Sci. Tech.* 6 031007-1-11.
- Berg, P., Promislow St., K., Pierre, J., Stumper, J., Wetton, B., 2004. Water management in PEM fuel cells. *J. Electrochem. Soc.* 151 (3), A341–A353.
- Chen, K.S., Hickner, M.A., Noble, D.R., 2005. Simplified models for predicting the onset of liquid water droplet instability at the gas diffusion layer/gas flow channel interface. *Int. J. Energy Res.* 29 (12), 1113–1132.
- Dullien, F.A., 1992. *Porous Media: Fluid Transport and Pore Structure* 2nd ed. Academic Press, New York, pp. 373–378.
- He, G., Ming, P., Zhao, Z., Abudula, A., Xiao, Y., 2007. A two-fluid model for two-phase flow in PEMFCs. *J. Power Sour.* 163 (2), 864–873.
- Jiao, K., Zhou, B., Quan, P., 2006. Liquid water transport in parallel serpentine channels with manifolds on cathode side of a PEM fuel cell stack. *J. Power Sour.* 154 (1), 124–137.
- Kandlikar, S.G., Lu, Z., Lin, T.Y., Cooke, D., Daino, M., 2009. Uneven gas diffusion layer intrusion in gas channel arrays of proton exchange membrane fuel cell and its effects on flow distribution. *J. Power Sour.* 194 (1), 328–337.
- Knights, S.D., Colbow, K.M., St-Pierre, J., Wilkinson, D.P., 2004. Aging mechanisms and lifetime of PEFC and DMFC. *J. Power Sour.* 127 (1–2), 127–134.
- Maharudrayya, S., Jayanti, S., Deshpande, A.P., 2005. Flow distribution and pressure drop in parallel-channel configurations of planar fuel cells. *J. Power Sour.* 144 (1), 94–106.
- Quan, P., Lai, M., 2007. Numerical study of water management in the air flow channel of a PEM fuel cell cathode. *J. Power Sour.* 164 (1), 222–237.
- Rapaport, P., Lai, Y., Ji, C., 2006. GDM intrusion into reactant gas channels and the effect on fuel cell performance. In: *The Fourth International Conference on Fuel Cell Science and Technology*, Irvine, California.
- Shimpalee, S., Greenway, S., Van Zee, J.W., 2006. The impact of channel path length on PEMFC flow-field design. *J. Power Sour.* 160 (1), 398–406.
- St-Pierre, J., Wong, A., Diep, J., Kiel, D., 2007. Demonstration of a residence time distribution method for proton exchange membrane fuel cell evaluation. *J. Power Sour.* 164 (1), 196–202.
- St-Pierre, J., Jia, N., Rahmani, R., 2008. PEMFC contamination model: competitive adsorption demonstrated with NO₂. *J. Electrochem. Soc.* 155, B315–B320.
- Wang, C.Y., Groll, M., Rosler, S., Tu, C.J., 1994. Porous medium model for two-phase flow in mini channels with applications to micro heat exchangers. *Heat Rec. Sys. CHP* 14 (4), 377–389.
- Wang, C.Y., Cheng, P., 1996. A multiphase mixture model for multiphase, multicomponent transport in capillary porous media—I: model development. *Int. J. Heat Mass Transfer* 39, 3607–3618.
- Wang, Z.H., Wang, C.Y., Chen, K.S., 2001. Two-phase flow and transport in the air cathode of proton exchange membrane fuel cells. *J. Power Sour.* 94 (1), 40–50.
- Wang, X., Duan, Y., Yan, W., 2007. Numerical study of cell performance and local transport phenomena in PEM fuel cells with various flow channel area ratios. *J. Power Sour.* 172 (1), 265–277.
- Wang, Y., Basu, S., Wang, C.Y., 2008. Modeling two-phase flow in channels of a polymer electrolyte fuel cell. *J. Power Sour.* 179, 603–617.
- Wilkinson, D., St-Pierre, J., 2003. In-plane gradients in fuel cell structure and conditions for higher performance. *J. Power Sour.* 113 (1), 101–108.
- Yang, X.G., Zhang, F.Y., Lubawy, A., Wang, C.Y., 2004. Visualization of liquid water transport in a PEFC. *Electrochem. Solid-State Lett.* 7, A408–A411.
- Yoon, Y., Lee, W., Park, G., Yang, T., Kim, C., 2004. Effects of channel configurations of flow field plates on the performance of a PEMFC. *Electrochim. Acta* 50 (2–3), 709–712.
- Yuan, J., Sunden, B., 2004. Two-phase flow analysis in a cathode duct of PEFCs. *Electrochim. Acta* 50, 677–683.
- Zhang, F.Y., Wang, X.G., Wang, C.Y., 2006. Liquid water removal from a polymer electrolyte fuel cell. *J. Electrochem. Soc.* 153, A225–232.
- Zhang, L., Bi, H.T., Wilkinson, D.P., Stumper, J., Wang, H., 2008. Gas-liquid two-phase flow patterns in parallel channels for fuel cells. *J. Power Sour.* 183 (2), 643–650.
- Zhu, X., Sui, P.C., Djalili, N., 2008. Three-dimensional numerical simulations of water droplet dynamics in a PEMFC gas channel. *J. Power Sour.* 181 (1), 101–115.